JACS
JOURNAL OF THE AMERICAN CHEMICAL SOCIETY

ARTICLE

pubs.acs.org/JACS

Hyperfine-Shifted ^{13}C Resonance Assignments in an Iron−Sulfur Protein with Quantum Chemical Verification: Aliphatic C−H···S 3-Center−4-Electron Interactions

William M. Westler,[*,†] I-Jin Lin,[‡] András Perczel,[∥] Frank Weinhold,[§] and John L. Markley[*,†,‡]

[†]National Magnetic Resonance Facility at Madison, [‡]Department of Biochemistry, Graduate Program in Biophysics, and [§]Theoretical Chemistry Institute, Department of Chemistry, University of Wisconsin, Madison, Wisconsin 53706, United States

[∥]Laboratory of Structural Chemistry and Biology and Protein Modeling Group of HAS-ELTE, Institute of Chemistry, Eötvös Loránd University, Budapest, Hungary

Supporting Information

ABSTRACT: Although the majority of noncovalent interactions associated with hydrogen and heavy atoms in proteins and other biomolecules are classical hydrogen bonds between polar N−H or O−H moieties and O atoms or aromatic π electrons, high-resolution X-ray crystallographic models deposited in the Protein Data Bank show evidence for weaker C−H···O hydrogen bonds, including ones involving sp^3-hybridized carbon atoms. Little evidence is available in proteins for the (even) weaker C−H···S interactions described in the crystallographic literature on small molecules. Here, we report experimental evidence and theoretical verification for the existence of nine aliphatic (sp^3-hybridized) C−H···S 3-center−4-electron interactions in the protein *Clostridium pasteurianum* rubredoxin. Our evidence comes from the analysis of carbon-13 NMR chemical shifts assigned to atoms near the iron at the active site of this protein. We detected anomalous chemical shifts for these carbon-13 nuclei and explained their origin in terms of unpaired spin density from the iron atom being delocalized through interactions of the type: C−H···S−Fe, where S is the sulfur of one of the four cysteine side chains covalently bonded to the iron. These results suggest that polarized sulfur atoms in proteins can engage in multiple weak interactions with surrounding aliphatic groups. We analyze the strength and angular dependence of these interactions and conclude that they may contribute small, but significant, stabilization to the molecule.

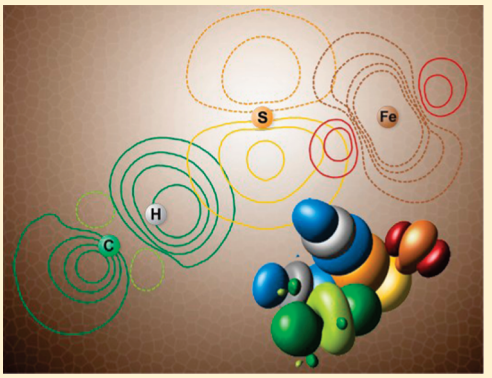

INTRODUCTION

The stability of proteins and other biomacromolecules is determined by weak interactions from hydrogen bonds, electrostatic interactions, hydrophobic effects, and van der Waals interactions. The proper formulation of the force fields that represent these interactions is required for accurate simulations of protein energetics, conformations, and dynamics.[1,2] Of these interactions, hydrogen bonds play a key role in determining the specificity of molecular interactions.[3] The presence of hydrogen bonds in proteins and nucleic acids generally is inferred from heavy-atom interatomic distances derived from high-resolution, single-crystal X-ray structural models; however, more recently, nuclear magnetic resonance (NMR) spectroscopy has been used as a more direct method for detecting hydrogen bonds and quantifying their strengths.[4] Although the majority of hydrogen bonds in proteins and other biomolecules are between polar N−H or O−H moieties and O atoms or aromatic π electrons, high-resolution X-ray crystallographic models deposited in the Protein Data Bank[5] show evidence for weaker C−H···O hydrogen bonds, including ones involving sp^3-hybridized carbon atoms.[6] Still weaker C−H···S "hydrogen bond"-like interactions, which are more accurately referred to as generic 3-center−4-electron (3c−4e) hypervalent interactions (useful reading on general 3c−4e interactions and their relationship to H-bonding can be found in sections 3.5 and 5.1 of ref 7), have been described in the crystallographic literature on small molecules,[8,9] but there is little evidence for their existence in proteins. The one relevant report was the observation of small couplings between metal ions and protons on an alanine methyl group separated by 10 bonds in ^{113}Cd (or ^{199}Hg)-substituted rubredoxin from *Pyrococcus furiosus*.[10] This effect was attributed to a "through space" *J*-coupling mediated by "direct overlap of the CH_3 orbitals and the ^{113}Cd and/or Cys-S orbital". Here, we report anomalous chemical shifts for eight assigned aliphatic ^{13}C nuclei in native *Clostridium pasteurianum* rubredoxin (*CpRd*). We attribute the origin of the unusual chemical shifts to electron spin−nuclear spin coupling transmitted through C−H···S 3c−4e interactions. These interactions are the type C−H···S−Fe, where S comes from one of the four cysteines that are bound covalently to the iron. We show that the hyperfine shifts can be reproduced from quantum chemical calculations based on the X-ray structure of *CpRd* rubredoxin,[11] and we present theoretical estimates for the

Received: June 4, 2010
Published: January 5, 2011

dx.doi.org/10.1021/ja1049059 | *J. Am. Chem. Soc.* 2011, 133, 1310–1316

strength of these interactions and the dependence of the hyperfine shift on bond angles and distances.

EXPERIMENTAL PROCEDURES

Protein Production and Labeling. The procedures used for protein production, uniform and selective labeling with ^{13}C and ^{15}N, iron center reconstitution, and protein purification have been described previously.[12,13]

NMR Spectroscopy. One-dimensional ^{13}C NMR spectra were collected on a Bruker DMX-500 MHz spectrometer with a Bruker 5 mm QNP probe, switchable for ^{19}F, ^{31}P, and ^{13}C. To suppress the diamagnetic signals and enhance the sensitivity of the paramagnetic signals, a one-pulse sequence with a short repetition time or SuperWEFT pulse sequence was applied.[14] $^{13}C[^{15}N]$ difference decoupling spectra were collected on a Bruker DMX-600 MHz spectrometer equipped with a 10 mm $^{13}C[^{1}H, ^{15}N]$ probe. Hyperfine-shifted resonances from amide nitrogen atoms were irradiated selectively, and changes in the ^{13}C spectrum indicated adjacent carbonyl carbons.[15] The ^{15}N decoupler was alternatively set to the frequency of the target amide nitrogen atom and to a region of the spectrum with no signals. Subtraction was carried out automatically in the pulse program to remove all the unchanged signals. $^{13}C[^{13}C]$ constant time correlation spectra (CT-COSY) were collected on a Bruker DMX-500 MHz spectrometer with a Bruker 5 mm QNP probe. To resolve diamagnetic signals, the CT-COSY constant time was set to 8 ms. To resolve hyperfine-shifted signals and to suppress the diamagnetic signal, we used a pulse sequence with a SuperWEFT element ($180-\tau-90$) followed by the CT-COSY sequence (SW-CT-COSY experiment); the constant time was set to 4 ms to avoid the loss of the rapidly relaxing paramagnetic signals.[16]

Hyperfine Chemical Shift Calculations. The hyperfine shift computations utilized a 209-atom model derived from the 1.5 Å crystal structure of reduced *CpRd* (PDB code 1FHM).[11] The coordinates for the two heptapeptides at the metal site (residues 5−11 and 38−44 including all backbone and side chain heavy atoms) and the iron atom were extracted from the crystal structure. The N-termini were capped with acetyl groups, and the C-termini were capped with N-methyl groups. DS ViewerPro 5.0 from Accelrys Inc. was used to add hydrogens atoms to the structure. The coordinates for the protein model are supplied in XYZ format as Supporting Information (S1). The B3LYP/6-311++G (d,p) level of theory in Gaussian[17] was used in calculating the theoretical hyperfine chemical shifts. The Fermi contact spin densities were converted to shifts in ppm by using eqs 9 and 10 from a previous publication.[18] Mean diamagnetic chemical shifts from the BMRB database[19] (www.bmrb.wisc.edu) were used in comparing the experimentally observed chemical shifts with the computed hyperfine shifts. Natural bond orbital analysis was performed using NBO 5.0 (www.chem.wisc.edu/~nbo5). Computations were performed on a 12-processor SGI Altix computer, a 4 × 4 core processor AMD Opteron Supermicro server, and a 4 × 6 core processor Intel Xeon Supermicro server.

Computation of the Binding Energy for the CH_4−Fe(II)-$[SCH_3]_4$ Model Complex. The complex and the individual components were fully optimized at the B3LYP/6-311++G(d,p) and MPWB1K/6-311++G(d,p) levels of theory. Frequency calculations showed no imaginary frequencies, indicating that the complex and individual component models were in ground-state geometries. The complex was corrected for basis set superposition error (BSSE) by using the COUNTERPOISE keyword in Gaussian.[17] The computed BSSE was 0.25 and 0.28 kcal/mol for the B3LYP/6-311++G(d,p) and MPWB1K/6-311++G(d,p) levels of theory, respectively. The MPWB1K density functional has been shown to closely reproduce the accuracy of the more expensive MP2 and CCSD(T) levels of theory.[20] The implementation of the MPWB1K/6-311++G(d,p) functional in Gaussian was accomplished with the following keywords (comp.chem.umn.edu/info/DFT.htm): MBWP95/6-311++G(d,p) IOp(3/76=0560004400).

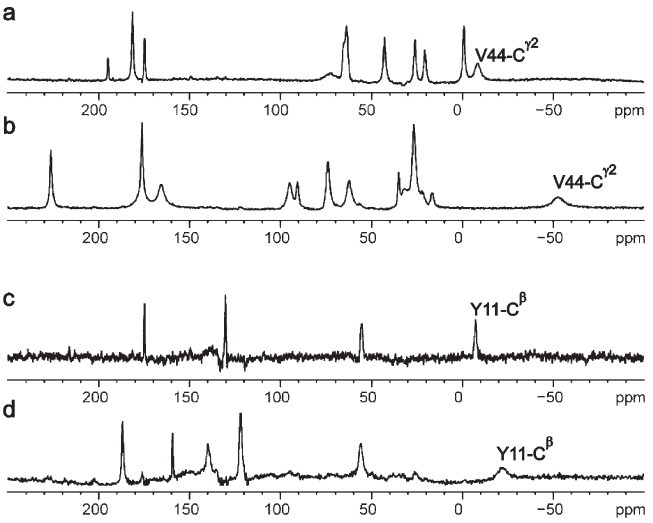

Figure 1. Example of selective labeling used in assigning the ^{13}C NMR signals from *Clostridium pasteurianum* rubredoxin with anomalous chemical shifts. (a) Reduced rubredoxin labeled with [U-13C]-valine. (b) Oxidized rubredoxin labeled with [U-13C]-valine. (c) Reduced rubredoxin labeled with [U-13C]-tyrosine. (d) Oxidized rubredoxin labeled with [U-13C]-tyrosine. The data collection method was optimized such that signals from nuclei close to the Fe−S center were observed preferentially in these spectra. The annotated ^{13}C signals have unusual chemical shifts when compared to the diamagnetic averages obtained from BMRB.[19] We attribute these large shifts to participation of these carbons and their attached hydrogens in 3c−4e interactions with sulfur atoms coordinated to iron: CH···S−Fe.

RESULTS

Anomalous Shifts. Carbon-13 NMR signals from *Clostridium pasteurianum* rubredoxin were assigned by methods involving selective isotope labeling (Figure 1).[13] These assignments revealed that resonances from eight sp^3-hybridized carbon atoms are shifted 20−80 ppm from their mean diamagnetic values listed in the BioMagResBank database;[19] all are more than 10 standard deviations from the mean diamagnetic chemical shift (Figure 2 and Table 1). Because rubredoxin contains a paramagnetic iron center, these unusual carbon chemical shifts certainly arise from hyperfine shifts caused by interactions of the nuclei with the unpaired electrons of the paramagnetic iron atom by either a through-space (pseudocontact) or a through-bond (contact) mechanism.[21] Table 1 also contains the chemical shifts determined for these atoms in the Zn^{2+}-substituted *CpRd*[22] showing that the resonances in the diamagnetic protein are not unusually shifted. The magnitude of each shift detected in Fe(II) *CpRd*, shown in Figure 2, is too large to be explained by the pseudocontact mechanism: calculations based on the known orientation and magnitude of the magnetic susceptibility tensor[23] yielded pseudocontact shifts less than 5.0 ppm for carbons in reduced rubredoxin and less than 1.3 ppm for carbons in oxidized rubredoxin. The contact mechanism drops off exponentially across successive bonds, and because all of the ^{13}C atoms with anomalous shifts are 6−11 covalent chemical bonds distant from the iron atom (Figure 2), it is highly unlikely that the shifts originate from propagation of spin density via classical covalent bonds. Direct interaction of iron orbitals with the aliphatic

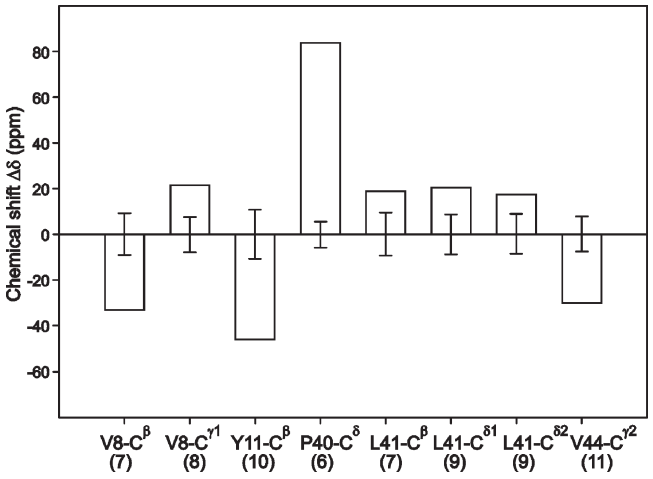

Figure 2. Deviations of eight assigned ^{13}C signals from reduced *Clostridium pasteurianum* rubredoxin from their mean diamagnetic chemical shifts. The error bars represent ±5 standard deviations from the mean diamagnetic shifts in BioMagResBank.[19] Residue and atom assignments are given along the abscissa. The total number of covalent bonds separating the iron atom and each carbon is shown in parentheses. The range of hyperfine shifts reported here corresponds to ^{13}C hyperfine coupling constants of approximately 0.02−0.1 MHz.

Table 1. Experimentally Observed and Calculated ^{13}C NMR Chemical Shifts for Reduced *Clostridium pasteurianum* Rubredoxin[a]

residue−carbon atom	experimental shifts[b]	calculated hyperfine shifts[c]
V8−C^{β}	−0.50 (30.88)	18.9
V8−$C^{\gamma 1}$	42.90 (21.91)	76.5
Y11−C^{β}	−6.70 (39.44)	−4.3
P40−C^{δ}	134.10 (50.68)	174.1
L41−C^{β}	61.00 (41.63)	51.4
L41−$C^{\delta 1}$	44.90 (24.83)	40.6
L41−$C^{\delta 2}$	41.40 (22.20)	26.4
V44−$C^{\gamma 2}$	−8.70 (21.43)	−134.6

[a] The hyperfine shifts are plotted in Figure 2. [b] Values in parentheses are the chemical shifts observed for these atoms in Zn^{2+}-substituted *Clostridium pasteurianum* rubredoxin[22] BMRB ID #5600. [c] The B3LYP/6-311++G(d,p) level of theory was used to calculate Fermi-contact hyperfine shifts; the values shown have been corrected for the average diamagnetic shifts obtained from BMRB.

carbons is also a possibility;[24] however, the through-space distances between the CH moieties and the Fe atom are quite long (>4 Å), making direct overlap unlikely. In addition, second-order perturbation energies obtained from NBO analysis[25] of the wave function show no direct interactions between iron orbitals and the CH bonds. As reported earlier,[18] the contact mechanism also propagates across hydrogen bonds, as illustrated by ^{15}N hyperfine shifts affected by ^{15}N−H···S−Fe hydrogen bonds. Thus, we propose here that weak 3c−4e interactions between aliphatic CH groups and the cysteine S^{γ} atoms provide the pathways for unpaired spin delocalization onto the carbon atoms. This mechanism is also consistent with the earlier observation[10] of long-range nuclear spin−nuclear spin scalar coupling between aliphatic protons and the NMR-active metal atom in cadmium- and mercury-substituted *Pyrococcus furiosus* rubredoxins.

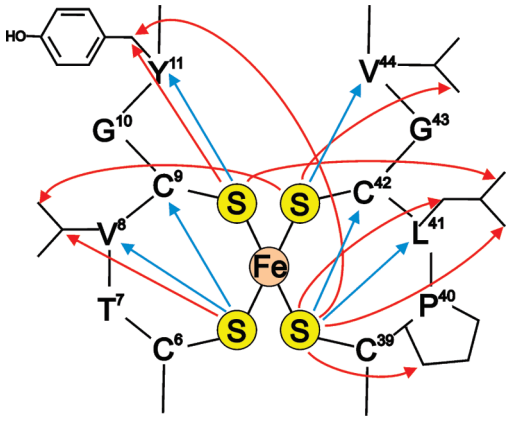

Figure 3. Schematic representation of hydrogen bonds and 3c−4e interactions at the active site of *Clostridium pasteurianum* rubredoxin. The C−H···S 3c−4e interactions reported here (red arrows) were detected by 3c−4e Fermi-contact shifts on ^{13}C. The N−H···S hydrogen bonds (blue arrows) were detected previously[31] by trans-hydrogen-bond Fermi-contact effects on ^{15}N chemical shifts.

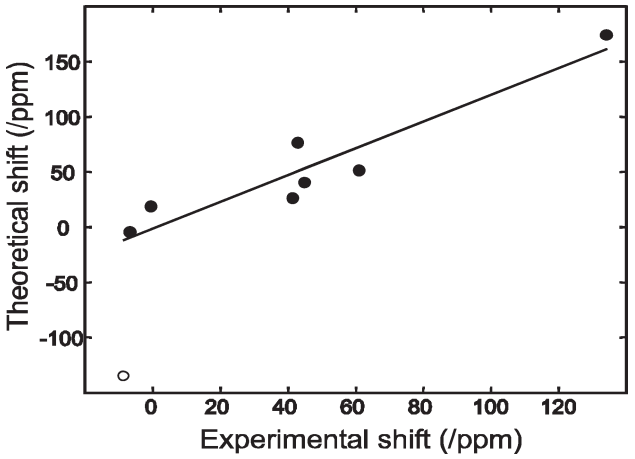

Figure 4. Robust linear regression fit of the DFT theoretical versus experimental chemical shifts (Table 1) for the eight anomalously shifted ^{13}C NMR signals of rubredoxin identified in Figure 2. The outlier data point (○) had a small weight (5%) in the robust fit. All data represented by "●" had weights of greater than 90%. The squared regression coefficient of the fit, excluding the outlier, was R^2 = 0.98 (see text for more).

C−H···S Interactions. The 3c−4e interactions detected in reduced rubredoxin are indicated in Figure 3. Eight carbons participate in nine CH···S 3c−4e interactions (represented by red arrows): the two H atoms attached to Tyr11−C^{β} interact with two different Cys−S^{γ} atoms. Also shown are the six NH···S hydrogen bonds (blue arrows) reported previously.[16] The results demonstrate that each cysteinyl sulfur atom can accommodate multiple 3c−4e interactions: 1 CH and 2 NH for Cys6−S^{γ}, 2 CH and 1 NH for Cys9−S^{γ}, 4 CH and 2 NH for Cys39−S^{γ}, and 2 CH and 1 NH for Cys42−S^{γ}.

Comparison of Experimental and Calculated Chemical Shifts. To test the validity of our analysis of the anomalous carbon chemical shifts, we used density functional theory (DFT) at the B3LYP/6-311++G(d,p) level of theory to calculate Fermi-contact contributions on the basis of a structural model derived from a crystal structure of reduced *Clostridium pasteurianum*

dx.doi.org/10.1021/ja1049059 |*J. Am. Chem. Soc.* 2011, 133, 1310–1316

Table 2. Geometric,[a] Energy, and Hyperfine Parameters of the $Fe(SCH_3)_4$−Methane Complex for Structures Optimized with B3LYP and MPWB1K Model Chemistries

parameter	B3LYP/6-311++G(d,p)	MPWB1K/6-311++G(d,p)
Fe−S* (Å)$^{-1}$ [b]	2.44	2.43
S*−H*[b] (Å)$^{-1}$ [c]	2.88	2.81
S*−C^{Me} (Å)$^{-1}$	3.98	3.88
H*−C^{Me} (Å)$^{-1}$	1.09	1.09
Fe−S (others) (Å)$^{-1}$	2.42,2.42,2.44	2.41,2.41,2.43
H−C^{Me} (others) (Å)$^{-1}$	1.09,1.09,1.09	1.09,1.09,1.09
Fe−S*−H* (deg)$^{-1}$	162.3	178.2
S*−H*−C^{Me} (deg)$^{-1}$	174.6	169.9
Fe−S*−H*−C^{Me} (deg)$^{-1}$	−156.2	51.9
binding energy (kcal/mol)$^{-1}$	1.55	1.82
NBO second-order perturbation + steric exchange energies (kcal/mol)$^{-1}$	1.16	1.14
hyperfine shift (ppm)$^{-1}$	563	256 (584)[d]

[a] Coordinates for both $Fe(SCH_3)_4$−methane complexes in XYZ format are available in the Supporting Information (S3 and S4). [b] S* refers to the sulfur atom involved in the 3c−4e interaction. [c] H* refers to the hydrogen atom of methane involved in the 3c−4e interaction. [d] Hyperfine shift calculated using B3LYP at the MPWB1K-optimized geometry.

rubredoxin[11] (Protein Data Bank code 1FHM). This approach earlier proved successful in reproducing the ^{15}N NMR chemical shifts of the six hydrogen-bonded Fe−S···H−^{15}N units of rubredoxin.[18] Figure 4 is a robust linear regression, which uses an iteratively reweighted least-squares algorithm (MATLAB[26]), of the theoretical shifts versus the eight anomalous experimental ^{13}C chemical shifts. The analysis provides a clear interaction mechanism for the observed chemical shifts. The weighting factor in the robust fit for all of the "●" is greater than 90%, whereas the outlier designated by the "○" has a weight of 5%. The squared regression coefficient for the fit of the data, excluding the outlier, is 0.984. The slope and intercept are 1.21 and −1.12, respectively. The outlier arises from the Val44−$C^{\gamma 2}$ atom, which is on the surface of the protein; the deviation may indicate a difference between the solution and crystal structures. The small systematic differences between theory and experiment, as suggested by the nonunit slope in the linear regression, may have to do with the lack of flexibility of the core orbitals in the basis sets and the use of a single point in space (delta function) to determine the Fermi contact values at the nuclear positions. In the calculation of *J*-coupling constants, which, like hyperfine interactions, require the Fermi contact spin density at the nucleus, the core basis sets are routinely decontracted, and tight polarization functions are added. This approach would probably improve the accuracy of the hyperfine values obtained. The cusp of the wave function that is located at the atomic position is well-known to be poorly described through the use of Gaussian basis orbitals. More accurate results for the Fermi contact spin density might be achieved through the use an approach like that of Rassolov and Chipman,[27] which uses global operators that are less sensitive than a delta function to local errors in the wave function near the nuclei.

Dependence of C−H···S Interaction Strengths on Geometry. To estimate the strength of an optimal C−H···S 3-center−4-electron interaction, we carried out quantum chemical calculations on optimized models consisting of methane complexed via the sulfur atom of Fe(II) tetramethylthiolate. Geometry, energies, and other parameters of these models that were obtained with the use of two different density functionals are collected in Table 2. Coordinates in XYZ format of the models are included in the Supporting Information (S3 and S4). The calculations employed Gaussian 03 or Gaussian 09[17] at the B3LYP/6-311++G(d,p) and the MPWB1K/6-311++G(d,p) levels of theory. The counterpoise-corrected binding energy for the complex was 1.70 and 2.00 kcal/mol, respectively. As an estimate for the strength of the interaction, the second-order perturbation energy summed with the steric exchange energy obtained from the Natural Bond Orbital[25] analysis gave a binding energy estimate of 1.16 kcal/mol for the B3LYP/6-311++G(d,p) model and 1.14 kcal/mol for the MPWB1K/6-311++G(d,p) model. The contact shift (hyperfine coupling constant) calculated for the methane ^{13}C in this complex was 563 ppm (0.69 MHz) for B3LYP/6-311++G(d,p) and 256 ppm (0.37 MHz) for MPWB1K/6-311++G(d,p) [the hyperfine shift calculated using B3LYP on the MPWB1K-optimized geometry was 584 ppm]; these values are about an order of magnitude larger than the contact shifts observed for the eight anomalously shifted ^{13}C resonances in rubredoxin. This difference can be accounted for by the local geometry in rubredoxin, which is substantially suboptimal for the C−H···S interactions. DFT calculations showed a relatively strong dependence of the hyperfine shift on the CH···S angle as well as a moderate dependence on the S···H distance (Figure 5). The CH moieties in the protein have interactions with multiple S atoms and thus do not have unique angles and distances; therefore, these values are not included in Figure 5. By contrast, our previous investigation of Fe−S···H−N hydrogen bonds[28,29] showed a strong dependence on the S···H distance but little dependence on the NH···S angle. A rough theoretical estimate of the strength of individual CH···S 3c−4e interactions in rubredoxin based on the magnitude of the Fermi contact interaction, assuming a simple linear relationship between the interaction strength and hyperfine coupling, is about one-tenth that calculated for the optimized structure. Even with such weak interactions, the nine CH···S 3c−4e interactions could contribute about as much as 1 kcal/mol of stabilization to the protein. However, the weakness of this interaction is exemplified by the lack of natural optimization of the geometry in the protein and might only be considered as a localized solvation of the cluster.

■ DISCUSSION

The unpaired electron density from the iron in rubredoxin provides a mechanism for direct detection of C−H···S−Fe

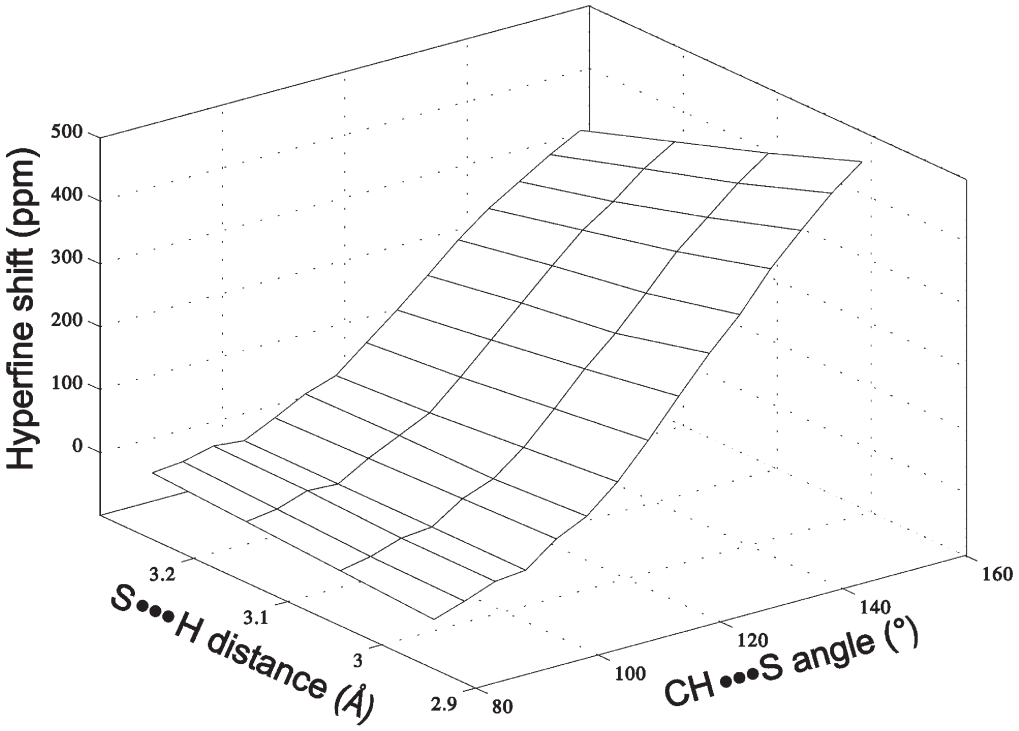

Figure 5. Plot of the dependence of the ^{13}C hyperfine shift of CH_4 on the S···H distance and the Fe−S···H angle in the CH_4−Fe(II)$[SCH_3]_4$ complex. The angle and distance were varied systematically; these values were fixed, and all other degrees of freedom were optimized at each point. The level of theory for optimization was B3LYP/6-31+G(d). The hyperfine shifts were calculated from the partially optimized structures at the B3LYP/6-311G(d,p) level of theory.

interactions in the form of hyperfine ^{13}C chemical shifts. The observed chemical shifts are consistent with quantum chemical (DFT) calculations of the same kind used to analyze NMR *J*-couplings and other electron spin−nuclear spin couplings.[18] Natural bond orbital (NBO) methods[25] provide a means of analysis of the energetics and orbital overlaps that are responsible for the observed Fermi contact effects.[18] The natural bond orbitals and natural atomic orbitals along with their occupancies are, in principle, an exact representation of the wave function. The atomic basis set of the converged wave function is recast into a complete orthonormal "natural minimal basis set" with high occupancy and a "natural Rydberg basis set" with low occupancy. The NBO representation allows for facile visualization of the orbital interactions involved in the C−H···S 3-center−4-electron interaction. NBO second-order perturbation analysis[7] shows that the contributors to the nonclassical transfer of spin density from the Fe−S center to aliphatic CH moieties are $\sigma_{Fe-S} \rightarrow \sigma_{CH}^*$ and S lone pair $n_S \rightarrow \sigma_{CH}^*$ interactions. On the right side of Figure 6, an example of the latter interaction is depicted by contour plots of pre-NBOs, which are NBOs prior to interatomic orthogonalization, showing the overlaps between orbitals. A lone pair orbital of the sulfur (n) is spin polarized through overlap with an unfilled Fe β d orbital ($n_S \rightarrow d_{Fe}^*$); that is, beta electrons from the S lone pair transfer into the unoccupied Fe β d-orbital. Electrons from the now α-spin enriched S lone pair then flow into the overlapping antibonding CH orbital ($n_S \rightarrow \sigma_{CH}^*$). The spin polarization is thus transmitted from the unoccupied Fe β d-orbital through the S lone pair to the antibonding CH orbital, which, in turn, places spin density on the atoms involved in the associated CH bonding orbital (σ_{CH}). This mechanism is fundamentally identical to the much stronger transfer of spin polarization from the Fe−S center to NH moieties that are hydrogen bonded to the sulfur atoms discussed previously.[18] A table of natural atomic orbital occupancies for the Fe atom in the CH_4−Fe(II)$[SCH_3]_4$ model complex at the B3LYP/6-311++G(d,p) level of theory is supplied in the Supporting Information (S2).

The calculated strength of the optimized CH···S interaction in the model Fe(II) tetramethylthiolate·methane is an order of magnitude larger than binding energies calculated for C−H···S hydrogen-bonded systems not containing metal atoms.[9] The polarization of iron-bound sulfur apparently strengthens the interaction. The B3LYP functional was not designed to describe long-range interactions. Density functionals such as those proposed by Truhlar[20] are designed to more accurately describe long-range and weak interactions and should improve the quality of the hyperfine calculations without the need to go to the computationally expensive model chemistries such as MP2 or CCSD(T). We have found that the binding energy obtained from a computation using B3LYP is very similar to that of MPWB1K, which is a functional designed to capture the long-range interactions.[20] Both calculations are in rough agreement with the binding energy obtained from NBO analysis through the sum of the second-order perturbation and steric exchange energies.

The stronger NH···S hydrogen bonds in rubredoxin[28] appear to dominate the hydrogen-bonding network; they have close to optimal geometries, whereas the CH···S 3c−4e interactions with suboptimal geometries apparently serve to adventitiously solvate the iron−sulfur center. Our previous study of rubredoxin mutants showed that associated changes in reduction potentials can be explained largely in terms of effects on the strengths of the six NH···S hydrogen bonds in the oxidized and

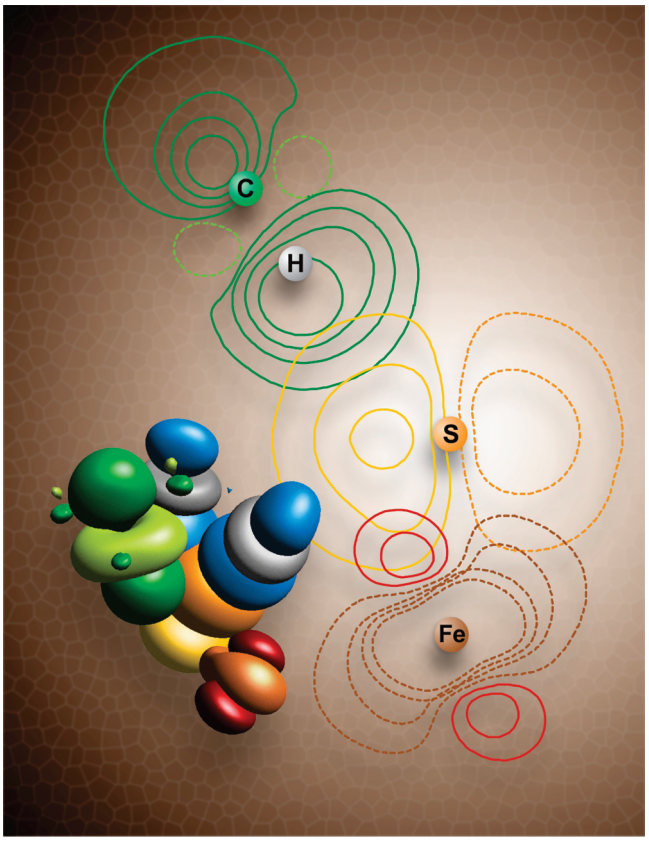

Figure 6. Three-dimensional representation of the natural bond orbitals (NBOs) for hydrogen bonds to the sulfur atom of one of the four cysteine residues (cysteine-6) that coordinate the iron atom of rubredoxin (left). The antibonding iron d-orbital is in red and rust; the sulfur lone pair p-orbital is in yellow and orange. Shown are antibonding orbitals of one carbon−hydrogen 3c−4e interaction (green, valine-8 C^{β}−H) and two nitrogen−hydrogen bonds (blue, valine-6 N−H and cysteine-9 N−H) that are involved in bonding interactions with the sulfur lone pair. The figure is based on the spin densities extracted[18] from a Gaussian 03[17] calculation on the 209-atom model derived from the 1.5 Å crystal structure of reduced *CpRd* (PDB code 1FHM). The contour plot shows the overlap of orbitals involved in the 3e−4c interaction referred to in this publication (right). The contour plot was created with NBOView 1.0,[32] and the space-filling model was produced with gOpenMol[33,34] from a Gaussian 03[17] cube file.

reduced states.[29] The weak 3c−4e interactions of CH···S moieties may serve to protect the redox potential of the Fe−S center from the effects of solvating water. Beyond this, these 3c−4e interactions may assist in the transfer of electrons by "displaying" the electron at the surface of the protein to partners during redox reactions. Similar to long-range electron transfers seen in other redox reactions,[30] the delocalization of the wave function to the aliphatic CH moieties acts as a "short circuit" for the electrons over the distance from the iron atom to the protein surface and could potentially be a mechanism to increase the kinetic rate of electron transfer by reducing the transition state energy.

■ ASSOCIATED CONTENT

Supporting Information. (S1) Coordinates in XYZ format are supplied for the reduced *CpRd* model used in the computations; (S2) a table of natural atomic orbital occupancies for the Fe atom in the CH_4−Fe(II)$[SCH_3]_4$ model complex [B3LYP/6-311++G(d,p)]; (S3) coordinates in XYZ format for the B3LYP/6-311++G(d,p) geometry-optimized CH_4−Fe(II)$[SCH_3]_4$ complex; (S4) coordinates in XYZ format for the MPWB1K/6-311++G(d,p) geometry-optimized CH_4−Fe(II)$[SCH_3]_4$ complex; and (S5) complete ref 17. This material is available free of charge via the Internet at http://pubs.acs.org.

■ AUTHOR INFORMATION

Corresponding Author
milo@nmrfam.wisc.edu; markley@nmrfam.wisc.edu

■ ACKNOWLEDGMENT

This work was supported by the NIH Institute of General Medical Sciences (GM58667, J.L.M.). NMR data were collected at the National Magnetic Resonance Facility at Madison (NMRFAM), which is supported by a grant from NIH National Center for Research Resources (P41 RR02301). A.P. participated in this project at NMRFAM while visiting on a Fulbright Fellowship. We thank H. Adam Steinberg for assistance in creating the graphics.

■ REFERENCES

(1) Ponder, J. W.; Case, D. A. *Adv. Protein Chem.* **2003,** *66*, 27.
(2) Weinhold, F. *Adv. Protein Chem.* **2006,** *72*, 121.
(3) Jeffrey, G. A. *An Introduction to Hydrogen Bonding*; Oxford University Press: New York, 1997.
(4) Grzesiek, S.; Cordier, F.; Dingley, A. J. *Methods Enzymol.* **2001,** *338*, 111.
(5) Berman, H. M.; Henrick, K.; Nakamura, H.; Markley, J. L. In *Structural Bioinformatics*, 2nd ed.; Gu, J., Bourne, P., Eds.; John Wiley: New York, 2009; p 293.
(6) Manikandan, K.; Ramakumar, S. *Proteins* **2004,** *56*, 768.
(7) Weinhold, F. a.; Clark, L. *Valency and Bonding: A Natural Bond Orbital Donor-Acceptor Perspective*; Cambridge University Press: New York, 2005.
(8) Taylor, R.; Kennard, O. *J. Am. Chem. Soc.* **1982,** *104*, 5063.
(9) Domagala, M.; Grabowski, S. J. *J. Phys. Chem. A* **2005,** *109*, 5683.
(10) Blake, P. R.; Lee, B. M.; Summers, M. F.; Adams, M. W. W.; Park, J. B.; Zhou, Z. H.; Bax, A. *J. Biomol. NMR* **1992,** *2*, 527.
(11) Min, T.; Ergenekan, C. E.; Eidsness, M. K.; Ichiye, T.; Kang, C. *Protein Sci.* **2001,** *10*, 613.
(12) Xia, B.; Pikus, J. D.; Xia, W.; McClay, K.; Steffan, R. J.; Chae, Y. K.; Westler, W. M.; Markley, J. L.; Fox, B. G. *Biochemistry* **1999,** *38*, 727.
(13) Lin, I. J.; Xia, B.; King, D. S.; Machonkin, T. E.; Westler, W. M.; Markley, J. L. *J. Am. Chem. Soc.* **2009,** *131*, 15555.
(14) Inubushi, T.; Becker, E. D. *J. Magn. Reson.* **1983,** *51*, 128.
(15) Cheng, H.; Westler, W. M.; Xia, B.; Oh, B. H.; Markley, J. L. *Arch. Biochem. Biophys.* **1995,** *316*, 619.
(16) Machonkin, T. E.; Westler, W. M.; Markley, J. L. *J. Am. Chem. Soc.* **2002,** *124*, 3204.
(17) Frisch, M. J.; et al. *Gaussian 03*; Gaussian, Inc.: Pittsburgh, PA, 2003.
(18) Wilkens, S. J.; Xia, B.; Weinhold, F.; Markley, J. L.; Westler, W. M. *J. Am. Chem. Soc.* **1998,** *120*, 4806.
(19) Seavey, B. R.; Farr, E. A.; Westler, W. M.; Markley, J. L. *J. Biomol. NMR* **1991,** *1*, 217.
(20) Zhao, Y.; Truhlar, D. G. *J. Phys. Chem. A* **2005,** *109*, 5656.
(21) Bertini, I.; Luchinat, C. *NMR of Paramagnetic Molecules in Biological Systems*; Benjamin/Cummings: Menlo Park, CA, 1986.
(22) Bougault, C. M.; Eidsness, M. K.; Prestegard, J. H. *Biochemistry* **2003,** *42*, 4357.

(23) Volkman, B. F.; Wilkens, S. J.; Lee, A. L.; Xia, B.; Westler, W. M.; Beger, R.; Markley, J. L. *J. Am. Chem. Soc.* **1999,** *121*, 4677.
(24) Doddrell, D.; Roberts, J. D. *J. Am. Chem. Soc.* **1970,** *92*, 6839.
(25) Reed, A. E.; Curtiss, L. A.; Weinhold, F. *Chem. Rev.* **1988,** *88*, 899.
(26) *MATLAB*, 5.2 ed.; The Mathworks, Inc.: Massachusetts, 2001.
(27) Chipman, D. M.; Rassolov, V. A. *J. Chem. Phys.* **1997,** *107*, 5488.
(28) Lin, I. J.; Gebel, E. B.; Machonkin, T. E.; Westler, W. M.; Markley, J. L. *J. Am. Chem. Soc.* **2003,** *125*, 1464.
(29) Lin, I. J.; Gebel, E. B.; Machonkin, T. E.; Westler, W. M.; Markley, J. L. *Proc. Natl. Acad. Sci. U.S.A.* **2005,** *102*, 14581.
(30) Gray, H. B.; Winkler, J. R. *Chem. Phys. Lett.* **2009,** *483*, 1.
(31) Xia, B.; Westler, W. M.; Cheng, H.; Meyer, J. P.; Moulis, J. M.; Markley, J. L. *J. Am. Chem. Soc.* **1995,** *117*, 5347.
(32) Wendt, M.; Weinhold, F., 2000.
(33) Bergman, D. L.; Laaksonen, L.; Laaksonen, A. *J. Mol. Graphics Modell.* **1997,** *15*, 301.
(34) Laaksonen, L. *J. Mol. Graphics* **1992,** *10*, 33.